Ab initio calculation of the core-hole effect in the electron energy-loss near-edge structure

Shang-Di Mo and W. Y. Ching
Department of Physics, University of Missouri-Kansas City, Kansas City, Missouri 64110
(Received 25 April 2000)

A computational scheme to fully account for the core-hole relaxation effect in electron energy-loss near-edge structure has been successfully implemented. Results on α-Al_2O_3, MgO, and $MgAl_2O_4$ crystals have reproduced all experimental details in all 11 edges. This is achieved by including three essential elements in the calculation: (1) A correct description of the presence of the hole in the core state of the excited atom. (2) The interaction between the excited electron in the conduction band and the hole left behind. (3) Use of large supercell for the final-state calculation. To a lesser extent, the inclusion of dipole matrix elements between the initial ground state and the final core-hole state is also important for the relative intensity of the structures. It is shown that the wave function of the excited electron in the conduction band in the presence of the core-hole state is localized to within the second-nearest-neighbor atoms, and is significantly different from the conduction-band wave function obtained from the ground-state calculation.

I. INTRODUCTION

In recent years, electron energy-loss spectroscopy has evolved into a very useful tool for studying material properties at atomic level.[1] In particular, the energy-loss near-edge structure (ELNES) observed in the inner-shell ionization process is a powerful technique for material characterizations. It is similar to the x-ray-absorption near-edge structure (XANES). Generally speaking, XANES measurements can give a higher-energy resolution than ELNES measurements, but will require special facilities and associated instrumentation. The ELNES is more accessible, and can be obtained by using dedicated analytical transmission electron microscopy. With a realistic goal of having a sub-eV resolution, the ELNES spectra can show a rich variety of structures, which can be correlated to the structure and composition of the material under study. The so-called ''fingerprint'' approach is often used by looking for common features of the same ELNES edge in different compounds, and inferring the electronic or structural property.[2] With ELNES fingerprints, a quantitative determination of site occupancy, the chemical shift of a given element, as well as information on local bond lengths and bond angles are possible. Recently, the ELNES was used to characterize the interfacial states of {111} Cu-MgO interfaces,[3] to elucidate the chemical bonding in electron-irradiated graphite,[4] to investigate the role of oxygen in the intergranular amorphous layers in β-SiC,[5] to clarify the atomic-scale structure, segregation, and bonding at the grain boundaries in superplastic ceramics,[6] and to probe the electromagnetic near-field in nanoparticles.[7]

To properly interpret experimental ELNES edges, especially for complex materials of unknown structures, a theoretical calculation with sufficient predictive power is *sine qua non*. The fundamental theory for the ELNES was established a long time ago based on inelastic electron scattering theory.[8,9] Over the years, many ELNES calculations have been carried out on many crystals, using either a multiple-scattering approach,[10,11] or one-electron band theory,[12–14] or a molecular cluster calculation.[15] In the band-structure method, the site-projected local density of states (LDOS) from density-functional calculations is widely used to interpret the ELNES spectra.[13,14] However, the agreement between the calculated and measured spectra is not always as good as one would like to claim. There are several reasons for this disappointment. First, it is a common practice to align the major peak, which is usually the most dominating feature in a given spectrum. In other words, the actual transition energy is not a part of the calculation. This can sometimes result in a misassignment of the peak structures. Second, the intensity of both the calculated and measured spectra are in arbitrary units. They are adjusted to produce the best ''agreement.'' One of the major challenges in ELNES calculation is to reproduce the relative intensities of various peak structures, not just their positions. Third, limited experimental resolution and the broadening procedure applied to the theoretical curve tend to mask fine details, which could otherwise be significant. Also, sample impurity or contamination may introduce spurious structures in the measured spectra. Finally, it is not common to present calculated results for all the edges in a given compound, or the same edge in different compounds. A good agreement in one edge and in one material is not always accompanied by an equally good agreement of the other edges in the same compound, or the same edge in different compounds. Such selective presentations make an honest assessment of the success or failure of a particular method in ELNES analysis a rather difficult task.

In this paper, we show that superior agreement between measured and calculated ELNES spectra can be obtained as would be demonstrated in the 11 K and L edges in three oxides: MgO, α-Al_2O_3, and $MgAl_2O_4$. In Sec. II, we will outline the main reason for the difficulty to obtain superior agreements, namely, the neglect of the core-hole relaxation effect. We then describe a computational scheme that accounts for the core-hole effect. The results on the three crystals are presented and compared with the experimental data in Sec. IV. Some conclusions are presented in Sec. V.

II. CORE-HOLE EFFECT

The main reason for the poor agreement between theory and experiment of the ELNES spectra is the neglect of the core-hole effect, and to a lesser extent, the exclusion of the

matrix elements of transition in the calculation. The ELNES intensity $I(E)$, which is proportional to the differential cross section, can be expressed in terms of the macroscopic dielectric function $\varepsilon(q,\omega)$:[16]

$$I(E)\propto \frac{d^2\sigma}{d\Omega\, dE}\propto \mathrm{Im}\left\{\frac{-1}{\varepsilon(\omega)}\right\} \tag{1}$$

where the quantity $\mathrm{Im}\{-1/\varepsilon(\omega)\}=\varepsilon_2/(\varepsilon_1^2+\varepsilon_2^2)$ is the energy-loss function. At high energies, ε_1 is close to unity while ε_2 is small, and the energy-loss function can be written as[17]

$$\mathrm{Im}\left\{\frac{-1}{\varepsilon(\omega)}\right\}=\varepsilon_2(\omega)$$

$$=\frac{e^2}{m\pi\hbar\omega^2}\sum_f |\langle f|\vec{P}|i\rangle|^2\delta(\hbar\omega-E_f+E_i), \tag{2}$$

where $|i\rangle$ is the initial core state, $|f\rangle$ is the unoccupied final state in the conduction band (CB), and E_i and E_f are the respective energies of the states. $\vec{P}=-i\vec{\nabla}$ is the momentum operator, and $\hbar\omega$ is the transition energy. The final state is the one with an electron in the CB and a hole in the atomic core. The electron and hole can interact strongly, thereby modifying the final state to be drastically different from that of the ground-state calculation. If one ignores the core-hole relaxation effect and assumes a constant matrix element, $I(E)$ reduces to the site-specific LDOS in the CB region, subject to the dipole selection rule for the orbital quantum number. Thus the excitation of a $1s$ core electron (K edge) is interpreted by a p type LDOS and the excitation of a $2p$ core electron (L edge) is represented by the $(s+d)$ components of the LDOS in the CB.

The theory of a core exciton in semiconductors was established about two decades ago.[18] It was also realized that many-body effect may play an important role,[19] especially when the perturbation by the core-hole potential is significant. Nevertheless, in extreme cases when a single-photon electron either makes a transition into an initially empty shell or fills the shell, the near-edge x-ray absorption or the electron energy loss can be reduced to a single-particle problem. Various attempts have been made to account for the core-hole effect in the ELNES (Refs. 20–25) and XANES.[26,27] A popular approach is to replace the excited atom by the next element in the Periodic Table to simulate the absence of a core electron, or the so-called $Z+1$ approximation.[20,21,23,24,27] In particular Lie and co-workers[23,24] indicated that the presence of the core hole must be considered in order to reproduce the experimental features. They calculated the core-hole effect using a full-potential linear-augmented plane-wave method with a $Z+1$ supercell approximation. The results on the B-K edges in TiB_2 and AlB_2 are in good agreement with experiment. However, there are many different ways to implement the $Z+1$ approach. The most common one is to use the $Z+1$ calculation for the electronic structure and use the results of the LDOS for interpretation, and this may not result in an improvement over the simple LDOS. As will be shown later below, the ELNES measures a single ion excitation. A large supercell must be used to correctly describe the electron-core hole interaction, whether using a $Z+1$ approximation or a more rigorous scheme. This was rarely the case in previous studies. Another method that has been used effectively to account for the core-hole relaxation is to use the Slaters' transition state in conjunction with a large-cluster molecular-orbital calculation.[15] The ELNES spectrum is represented by the LDOS of a transition state in which the core state of the central atom has only a $\frac{1}{2}$ electron occupation, with the other $\frac{1}{2}$ electron placed at the lowest unoccupied molecular orbitals (LUMO's).[15,25] An advantage of this approach is the relative energy of the core state and the half-occupied LUMO state gives some qualitative estimation of the leading ELNES peak. Strictly speaking, the core-hole effect is a two-particle interaction between an electron in the unoccupied CB and a hole in the core. They interaction must be accounted for, and separate calculations of the initial and final states are necessary.

III. IMPLEMENTATION OF CORE-HOLE EFFECT WITHIN THE OLCAO BAND METHOD

The orthogonalized linear combination of atomic orbital (OLCAO) method is a density-functional-theory-based *ab initio* all-electron band-structure method.[28] One of the attractive features of this method is the atomic description of the basis function in the expansion, which makes the decomposition of the density of states into local atomic components a natural and unambiguous task. The core states can be eliminated from the final secular equation by an orthogonalization-to-the-core process, which can significantly reduce the computational burden for large systems.[28] Over the years, the OLCAO method has been extensively used to study the electronic structure and optical properties of many inorganic crystals as well as their defect structures.[29–34] In particular, the LDOS obtained from the OLCAO calculation has been used to interpret the ELNES spectra of several oxides including grain boundary structures.[14,29,31,33] The LDOS result has only limited success in the interpretation of the ELNES spectra, for reasons stated above. However, the method is ideal for a rigorous inclusion of the core-hole effect in the ELNES calculation, upon which we will elaborate below. First, the initial and final states are calculated separately on supercells of sufficient size. In the supercell, the core states of the excited atom are retained in the basis set, while those of other atoms are eliminated by the orthogonalization process.[28] This flexible scheme is particularly advantageous, since a large supercell can be used for electron-hole interaction without being computationally burdensome. A supercell that is too small is undesirable because the excited atom may interact with its image in the adjacent cells. The initial state is just the usual ground-state calculation on the supercell. The final state is obtained by removing one electron from the core of the target atom, and placing it at the lowest CB. The interaction between the excited electron and the hole left behind is fully accounted for by self-consistent iterations of the Kohn-Sham equations in the final state. The calculation is thus similar to that of an impurity atom (here represented by an excited atom) in a supercell. The ELNES spectra are obtained by direct evaluation of $I(E)$, including the full evaluation of the momentum matrix elements between the initial and final states. The difference in the total energy (TE) of the initial ground state and

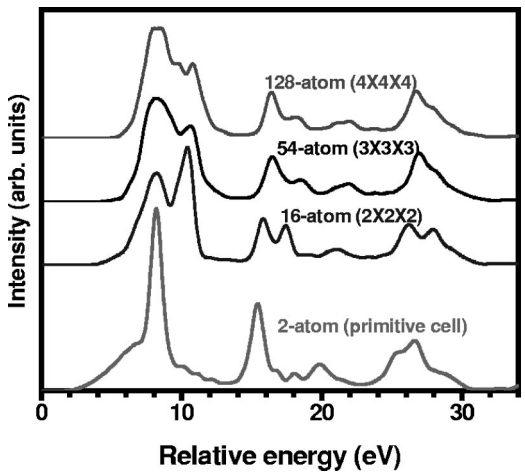

FIG. 1. Supercell size dependence of the O-*K* edge in MgO.

the final excited state is related to the experimental transition energy. A correction energy from the absorption edge to the major peak is added to the TE difference to obtain the theoretical peak position for the major ELNES peak. In this way, the transition energy of the electron excitation can also be estimated. This transition energy is different from the one obtained in the Slater transition-state approach,[15] which is the difference between the energies of the core state and the LUMO state from a single diagonalization.

To illustrate the importance of the supercell size, in Fig. 1 we show the size dependence of the O-*K* edge in MgO calculated using the scheme outlined above. The details of the spectra will be discussed in Sec. IV. The main point is that it takes a supercell of more than 100 atoms for the spectrum to converge. A small supercell contributes to the inaccuracy both in the peak positions and in the relative intensities of the peaks.

IV. RESULTS FOR THE *K* AND *L* EDGES IN MgO, α-Al_2O_3, AND $MgAl_2O_4$

We have applied the above scheme within the OLCAO method to calculate the ELNES spectra of the 11 *K* and *L* edges in three oxides, MgO, α-Al_2O_3, and $MgAl_2O_4$. Our intention is to make a systematic investigation and to see if the ELNES fingerprint technique is really hopeful or hopeless from the stand point of theoretical computation. These three crystals have the same cations in different coordinations and local environments, and hence very different ELNES spectra. Structural information about the three crystals is summarized in Table I. Furthermore, rather complete experimental data are available for comparison. After some tests, we decided to use supercells of 128, 120, and 112 atoms for MgO, α-Al_2O_3, and $MgAl_2O_4$, respectively, which should give sufficient accuracy. To achieve high resolution, 27 *k* points in the Brillouin zone of the supercell were used for *k*-space integration. In an earlier attempt, Lindner *et al.* studied the core-hole effect for the *K* edge in MgO using the $Z+1$ approximation within the multiple-scattering approach, but not the *L* edge.[21] They contended that for *L*-edge absorption, the presence of the core hole can be neglected; thus the $Z+1$ approximation should not apply. Ogasawara and coworkers analyzed the core-hole effect in the cation $L_{2,3}$ edge

TABLE I. Local bonding configurations in MgO, α-Al_2O_3, and $MgAl_2O_4$. Note that the lattice constants used were the optimized one using the LDA total-energy calculation, and may be slightly different from the experimental values.

Crystal	MgO	α-Al_2O_3	$MgAl_2O_4$.
Space group	$Fm3m$	$R3c$	$Fd3m$
Lattice constants (Å)	$a=4.213$	$a=5.128$	$a=8.086$
		$\alpha=55.333°$	
Cation coordination	6	6	4 for Mg
			6 for Al
Cation-O bond length (Å):			
Mg-O	2.1012(6)		1.919(4)
Al-O		1.969(3)	1.929(6)
		1.857(3)	
O coordination	4	4	4
O-cation bond length (Å)	2.1015(6)	1.969(2)	1.919(1)
		1.857(2)	1.929(3)

of MgO and α-Al_2O_3, based on discrete variational $X\alpha$ cluster calculations and a Slater transition-state approach.[15] They concluded that the core-hole effect in MgO is not significant, since their ground-state LDOS calculation could reproduce the experimental spectra reasonably well. On the other hand, they found that the strongest peak in the Al-$L_{2,3}$ edge in α-Al_2O_3 has its origin in the presence of the core hole. Recently, Köstlmeier and Elsässer calculated several ELNES edges in the same three crystals using a pseudopotential-mixed basis method.[13] The core-hole effect in the Mg-*K* edge was investigated by using a different construction of the on-site ionic pseudopotential to simulate the presence of the core-hole. Their calculated LDOS's exhibit the same peak positions and intensities as in the ground-state calculation, and were unable to reproduce the first spike near the onset. This is at least partly due to the use of small cell of only 8 atoms.

The 11 calculated ELNES edges in the three crystals, together with the available experimental data,[14,21,35,36] are presented in Figs. 2–6. The energy scale is set at the top of the valence band. The number on the experimental curve is the actual experimental value of the peak. The number on the theoretical curve is obtained as the difference in the TE between the initial- and final-state calculations, corrected for the shift in energy from the absorption threshold to the peak position. The differences between the two numbers in these spectra are quite small. It is gratifying to see that almost all the fine details of the peak positions and relative intensities in these spectra are reproduced by the calculation. This is in sharp contrast to the previous results based on the LDOS.[37] This is particularly impressive when one realizes that the edges of the same atom in different crystals are very different because of the different local environments. To our knowledge, the so-called spike structure in the Mg-*K* edge at 1310.2 eV (see Fig. 2) has never been successfully reproduced in the past.[13,15] We believe that the calculated Mg-*K* and Mg-$L_{2,3}$ edges for spinel $MgAl_2O_4$ are first-time theoretical results. The significantly different Mg edges in MgO and $MgAl_2O_4$ are obviously due to the fact that Mg in MgO is octahedrally coordinated, and Mg in $MgAl_2O_4$ is tetrahe-

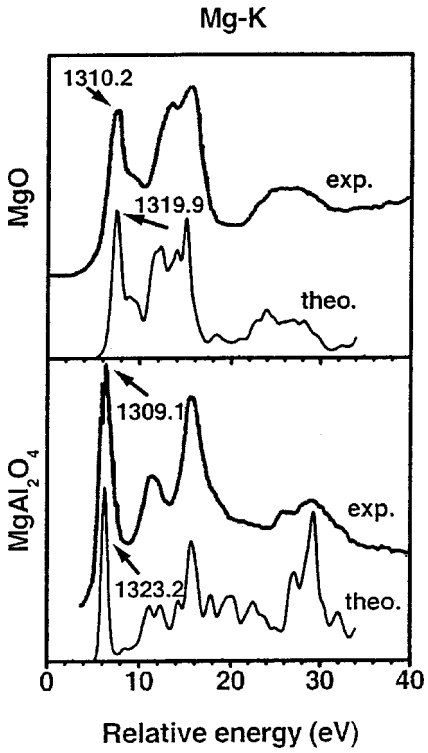

FIG. 2. Calculated and experimental Mg-*K* edges in MgO and $MgAl_2O_4$. The experimental data are from Ref. 21(MgO) and Ref. 36 ($MgAl_2O_4$).

drally coordinated. No experimental data for the Al-*K* edge in $MgAl_2O_4$ has been reported, to our knowledge, but our theoretical curves show different positions for the main peak. The Mg-*K* data in $MgAl_2O_4$ (Ref. 36) is from the XANES,

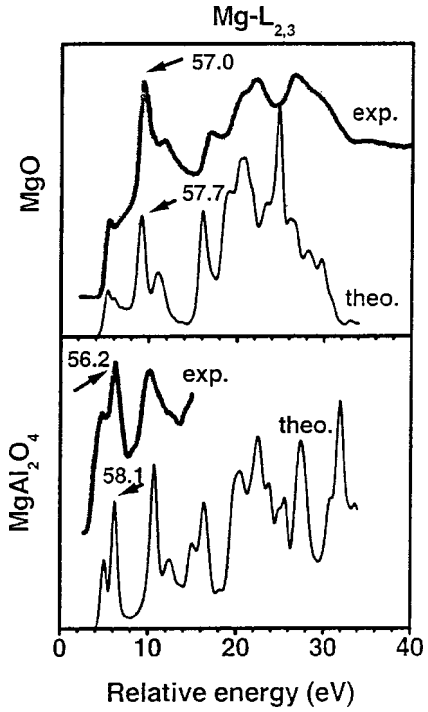

FIG. 3. Calculated and experimental Mg$L_{2,3}$ edges in MgO and $MgAl_2O_4$. The experimental data are from Ref. 21(MgO) and Ref. 35 ($MgAl_2O_4$).

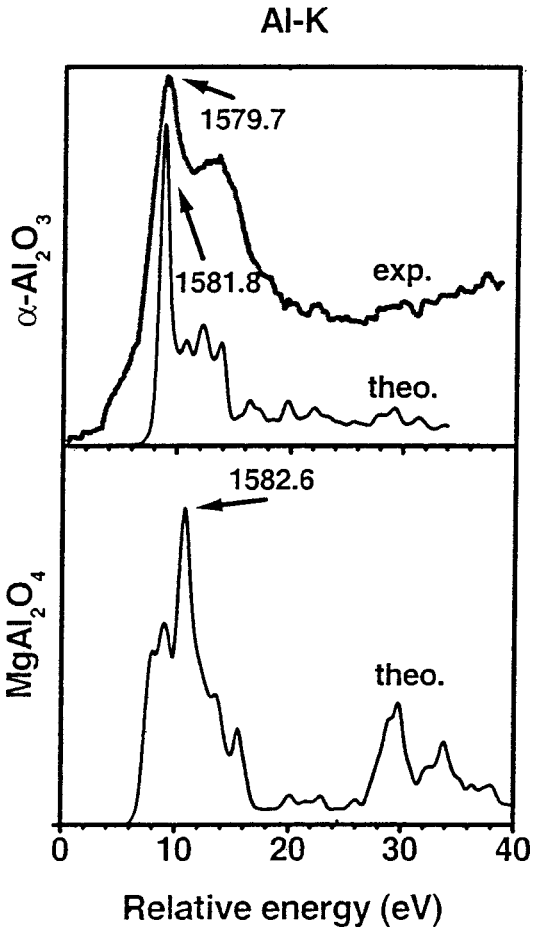

FIG. 4. Calculated and experimental Al-*K* edges in α-Al_2O_3 and $MgAl_2O_4$. The experimental data are from Ref. 14 (α-Al_2O_3). No experimental data were available for the Al-*K* edge in $MgAl_2O_4$.

which has a better resolution. In the case of O-*K* edges where the experimental resolution appears to be poor, the calculation provides more detailed information than the experiment. The O-*K* edges in these oxides are also different, especially for the structures beyond the main peak.

The only discrepancy in these comparisons appears to be that the experimental peak at 80.5 eV in the Al-$L_{2,3}$ edge of $MgAl_2O_4$ in Fig. 5 is much more pronounced than in the theoretical curve. This is most likely due to the fact that the experimental data on $MgAl_2O_4$ were collected on a natural mineral sample, which contains a certain fraction of inverse spinel.[35] In the inverse spinel, Al ions occupy both the octahedral (Al_{oct}) and tetrahedral (Al_{tet}) sites, while in the normal spinel Al ions occupy only the Al_{oct} sites. In $Y_3Al_5O_{12}$, both Al_{oct} and Al_{tet} sites are present. There is strong evidence that Al_{tet} has a stronger peak and is at a higher energy than Al_{oct}.[14] Thus the enhanced peak at 80.5 eV in the experimental Al-$L_{2,3}$ edge is most likely due to the presence of Al_{tet} in the natural mineral sample.

To illustrate the different hierarchy of the ELNES calculations, in Fig. 7 we show the Mg-*K* and Mg-$L_{2,3}$ edges in MgO obtained from four different levels of calculation with increasing sophistication. Figure 7(a) shows the ground-state LDOS involving no core states.[37] Figure 7(b) shows a photoabsorption cross section (PACS) calculation in which the matrix elements of transition between the core and the CB

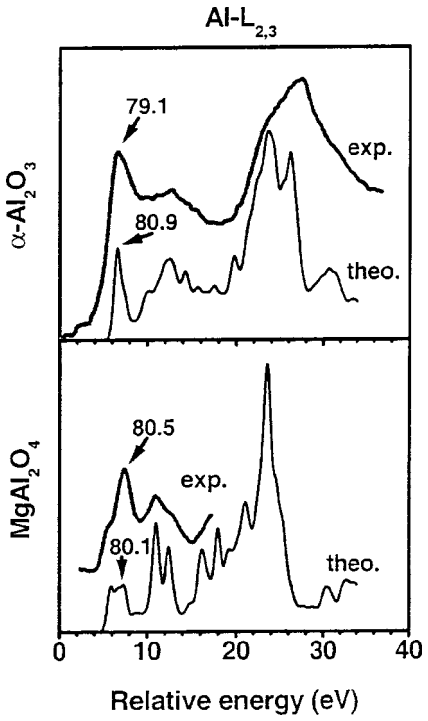

FIG. 5. Calculated and experimental Al-$L_{2,3}$ edges in α-Al_2O_3 and $MgAl_2O_4$. The experimental data are from Ref. 14 (α-Al_2O_3) and Ref. 35 ($MgAl_2O_4$).

states are included but with no core-hole interaction included. Figures 7(c) and 7(d) show the result of the $Z+1$ approximation and the result with a full inclusion of the core-hole effect, respectively. In these calculations, the initial and final states are calculated separately using a large supercell. The only difference between the two is that there is no actual hole in the core in the $Z+1$ approximation, so that there is no difference in the potential for a $1s$ electron excitation or a $2p$ electron excitation. We can see the following: (1) The LDOS is very different from the spectra with the core-hole effect included. (2) The PACS result is similar to the LDOS with slightly different relative peak intensities, reflecting the effect of the matrix elements. The difference is much larger for the L edge than for the K edge. (3) The $Z+1$ approach gives similar results to the full core-hole calculation for the Mg-K edge, but is less satisfactory for the Mg-$L_{2,3}$ edge. The intensity of the first peak in the Mg-$L_{2,3}$ edge is overestimated because of the difference in the screening effects for a $1s$ core hole and a $2p$ core hole. (4) The rigorous inclusion of the core-hole effect reproduces all the spectral details discussed above. These results clearly confirm the assertion that core-hole relaxation has the largest effect on the structures near the absorption edge. It should be emphasized that the main reason the present $Z+1$ approximation also yields superior agreement is because it is implemented in the same rigorous manner, using the same supercell, and including the matrix elements as in the rigorous specific core-hole calculation. The only difference is in the potential representation of the core of the excited atom.

Up to now, it is clear that a rigorous inclusion of the core-hole effect is crucial to a successful ELNES calculation. However, for most energy-band methods, the inclusion of transition matrix elements requires additional computational

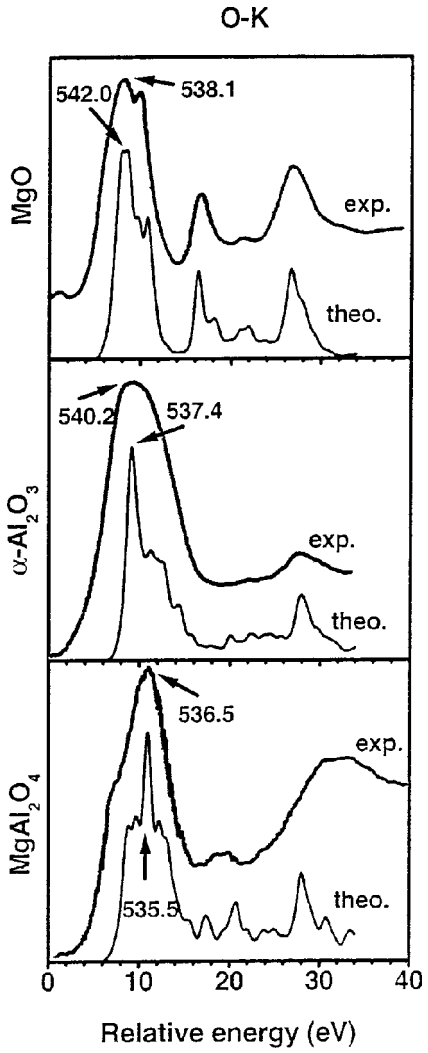

FIG. 6. Calculated and experimental O-K edges in MgO, α-Al_2O_5 and $MgAl_2O_4$. The experimental data are from Ref. 21 (MgO), Ref. 14 (α-Al_2O_3), and Ref. 35 ($MgAl_2O_4$).

effort, which may be onerous. In Fig. 7(e), we show the calculated LDOS of the final state, which includes the core-hole effect. Surprisingly, the resulting spectra are close to the more rigorous one with matrix elements included. In particular, they can produce the peak positions very well, but not the relative intensities of the peaks. This is quite evident in the 10–17-eV ranges for the Mg-K edge and in the first peak in the Mg-$L_{2,3}$ edge. We thus conclude that the inclusion of the transition matrix element is desirable for a better reproduction of the experimental spectra.

In Figs. 8 and 9, we display the square of the final-state wave functions in the CB for the Mg-K, Mg-$L_{2,3}$, and O-K edges in MgO. For comparison, the lowest CB state from the ground-state calculation and those obtained using the $Z+1$ approximation are also included. The figure in the (001) plane is Mg(O) centered for the Mg(O) edge. The wave function of the core-hole state extends to the region of nearest neighbors (NN's) for the Mg-K and Mg-$L_{2,3}$ edges, and to the second NN's for the O-K edge. They are somewhat more delocalized due to the presence of the core hole. The CB edge state from the ground-state calculation is essentially a very delocalized one. Also, the core-hole state wave func-

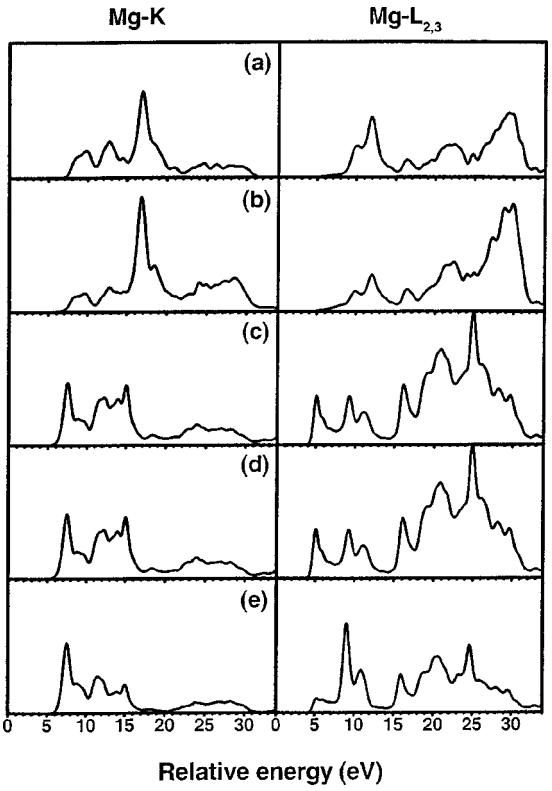

FIG. 7. Five different levels of the ELNES calculation for the Mg-K edge (left panel) and the Mg-$L_{2,3}$ edge (right panel) in MgO. (a) LDOS from ground-state calculation; (b) PACS calculation with matrix elements included; (c) $Z+1$ approximation; (d) full core-hole calculation; (e) LDOS from the final state of the core-hole calculation with no matrix elements included.

tions obtained from the $Z+1$ approximation are slightly different from the rigorous calculation, reflecting the approximation made in the $Z+1$ approach for the excited atom. Also, in the $Z+1$ approximation, no distinction between Mg-K and Mg-$L_{2,3}$ edges can be made. We have investigated the size of the core-hole states in the other two crystals, α-Al_2O_3 and $MgAl_2O_4$, with similar conclusions.

V. CONCLUSIONS

We have successfully implemented a rigorous scheme to account for the core-hole effect in the ELNES calculation within the *ab initio* OLCAO method. Application of this scheme to three crystals, MgO, α-Al_2O_3, and $MgAl_2O_4$, yield superior agreements on all 11 metal-K, metal-L, and O-K edges. All experimental features in these spectra are reproduced by the calculation. This is achieved by satisfying the three important components in the calculation. (1) The calculation must account for the presence of the hole in the core state of the excited atom. (2) The excited electron in the conduction band must be allowed to interact with the hole in the core. (3) A sufficiently large supercell must be used for the final-state calculation to avoid spurious interactions. The inclusion of the transition matrix elements is important if the relative intensities of the peaks in the spectra are to be reproduced. This has to be accomplished by separate calculations of the initial state (ground state) and the final state (an electron in the lowest CB in the presence of a core hole). It is also shown that the $Z+1$ approximation for the core-hole effect can provide very satisfactory results provided that the above conditions are met.

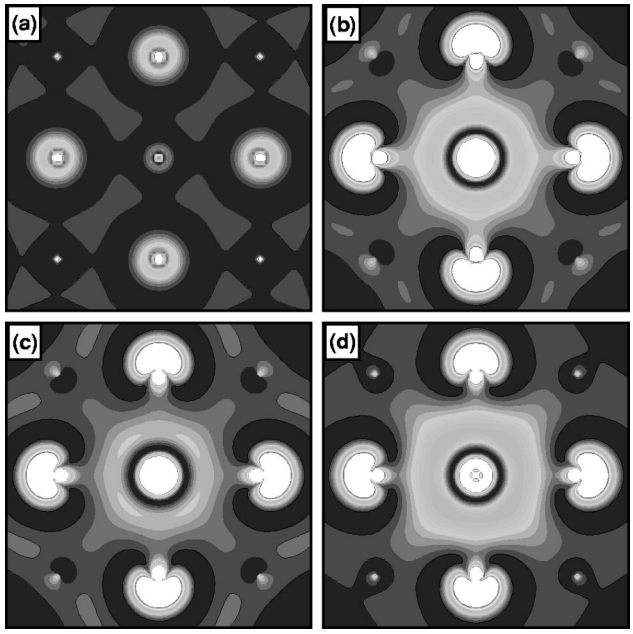

FIG. 8. $|\Psi(r)|^2$ of the lowest CB state in the supercell calculation for MgO on a (001) plane of the rocksalt structure. The center is at the Mg ion. The dark (white) shades represent region of low (high) density. The gray areas are regions of intermediate density. (a) Ground state calculation. (b) The same result obtained using the $Z+1$ approach. Note in the $Z+1$ approach, no distinction can be made between the Mg-1s or Mg-2p core excitation. (c) A Mg-1s core electron is excited to the lowest CB. (d) A Mg-2p core electron is excited to the lowest CB.

The present results provide great confidence in using the ELNES and XANES as fingerprint techniques for complex

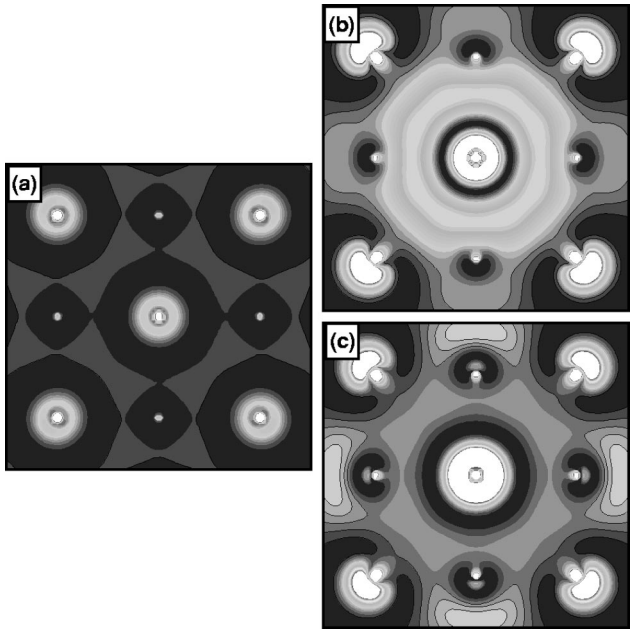

FIG. 9. Same as in Fig. 8 for the O-1s core electron excited to the lowest CB. The center is at the O ion. (a) Ground-state calculation. (b) Calculation using the $Z+1$ approach. (c) Core-hole calculation.

material characterizations. Preliminary calculations on ZnO,$SrTiO_3$,Y_2O_3,$Y_3Al_5O_{12}$, and other crystals yield equally impressive agreement, and will be reported elsewhere. It appears that the many-body effect in the ELNES spectra is not as important as originally envisioned, at least in the non-transition-metal oxides. This is quite surprising since, strictly speaking, the Kohn-Sham single-particle state in the unoccupied energy region has no physical meaning. Perhaps by allowing for the interaction between a core hole and an excited electron in the present scheme, an important step beyond the usual one-electron density-functional theory is already taken. It is hoped that with this computational scheme, a systematic interpretation of the ELNES spectra in many materials can be properly interpreted within the one-electron theory.

The crystals discussed so far are insulators. It is not clear to what extent the present method will be equally successful in metals, transition-metal oxides, and systems with strong electron-electron correlation. In these cases, a specific treatment of the many body effect will be necessary for ELNES and XANES, and for the theory of excited-state spectroscopy in general. In a strongly correlated electron system, two electrons may produce collective states,[38] whose implication on the spectroscopic properties is unknown. A many-body Green's, function method[39] or time-dependent density-functional theory[40] may have to be used. Such a treatment is clearly beyond the scope of the present paper.

ACKNOWLEDGMENTS

We thank Dr. Isao Tanaka for valuable discussion, and Dr. Y.-N. Xu for assistance. This research was supported by DOE Grant No. DE-FG02-84ER45170.

[1] See, for example, D. A. Muller, T. Sorsch, S. Moccio, F. H. Baumann, K. Evans-Lutterodt, and G. Timp, Nature (London) **399**, 758 (1999).
[2] R. Bryson, H. Sauer, and W. Fugel, in *Transmission Electron Energy Loss Spectroscopy in Materials Science*, edited by M. M. Disko, C. C. Ahn, and B. Fuitz (TMS, Warrendale, PA, 1992), p. 131.
[3] D. Imhoff, S. Laurent, C. Colliex, and M. Backhaus-Ricoult, Eur. Phys. J.: Appl. Phys. **5**, 9 (1999).
[4] S. Nuto *et al.* J. Appl. Phys. **38**, 1514 (1999).
[5] K. Kaneko, M. Yoshiya, I. Tanaka, and S. Tsurekawa, Acta Mater. **47**, 1281 (1999).
[6] Y. Ikuhara and T. Sakuma, Key Eng. Mater. **161**, 549 (1999).
[7] H. Cohen *et al.*, Phys. Rev. Lett. **80**, 782 (1998).
[8] R. F. Egerton, *Electron Energy Loss Spectroscopy in the Electron Microscope* (Plenum, New York, 1986).
[9] R. D. Leapman, P. L. Fejes, and J. Silcox, Phys. Rev. B **28**, 2361 (1983).
[10] V. Serin, C. Colliex, R. Brydson, S. Matar, and F. Boucher, Phys. Rev. B **58**, 5106 (1998); R. Brydson, J. Phys. D **29**, 1699 (1996).
[11] Z. Y. Wu, G. Ouvrard, P. Gressier, and C. R. Natoli, Phys. Rev. B **55**, 10 382 (1997).
[12] P. Rez, J. R. Alvarez and C. Pickard, Ultramicroscopy **78**, 175 (1999).
[13] S. Köstlmeier and C. Elsässer, Phys. Rev. B **60**, 14 025 (1999).
[14] M. A. Gülgün, W. Y. Ching, Y.-N. Xu, and M. Rühle, Philos. Mag. B **79**, 921 (1999).
[15] K. Ogasawara, I. Tanaka, and H. Adachi, Adv. Quantum Chem. **29**, 41 (1997); I. Tanaka and H. Adachi, Phys. Rev. B **54**, 4604 (1996).
[16] H. Raether, *Excitation of Plasmons and Interband Transitions by Electrons* (Springer-Verlag, New York, 1980).
[17] S.-D. Mo, Ph.D. dissertation, University of Missouri–Kansas City, 1998.
[18] H. P. Hjalmerson, H. Büttner, and J. D. Dow, Phys. Rev. B **24**, 6010 (1981).
[19] E. A. Stern and J. J. Reher, Phys. Rev. B **27**, 3351 (1986).
[20] M. M. Disko, J. C. H. Spence, O. F. Sankey, and D. Saldin, Phys. Rev. B **33**, 5642 (1986).
[21] T. Lindner, H. Sauer, W. Engel, and K. Kambe, Phys. Rev. B **33**, 22 (1986).
[22] R. Brydson, J. Bruley, and J. M. Thomas, Chem. Phys. Lett. **149**, 343 (1988).
[23] K. Lie, R. Brydson, and H. Davock, Phys. Rev. B **59**, 5361 (1999).
[24] K. Lie, R. Høier, and R. Brydson, Phys. Rev. B **61**, 1786 (2000).
[25] T. Mizoguchi, I. Tanaka, F. Oba, K. Ogasawara, and H. Adachi, Phys. Rev. B **61**, 2180 (2000).
[26] P. J. W. Weijs, H. J. M. Hendrix, R. A. de Grott, G. van der Laan, K. H. J. Burschow, G. Weich, and J. C. Fuggle, Phys. Rev. B **41**, 11 899 (1990).
[27] M. Nyberg, Y. Luo, L. Triguero, L. G. M. Petterson, and H. Agren, Phys. Rev. B **60**, 7956 (1999).
[28] W. Y. Ching, J. Am. Ceram. Soc. **73**, 3135 (1990).
[29] S. D. Mo and W. Y. Ching, J. Am. Ceram. Soc. **79**, 627 (1996); S.-D. Mo, W. Y. Ching, and R. H. French, J. Phys. D **29**, 1740 (1996); S.-D. Mo, W. Y. Ching, M. Chelshim, and G. Guscher, Phys. Rev. B **60**, 2416 (1999).
[30] D. Li and W. Y. Ching, Phys. Rev. B **54**, 13 616 (1996); W. Y. Ching, Y.-N. Xu, and Z.-Q. Gu, *ibid.* **54**, R15 585 (1996).
[31] S.-D. Mo, Y.-N. Xu, and W. Y. Ching, J. Am. Ceram. Soc. **80**, 1193 (1997); S.-D. Mo and W. Y. Ching, Phys. Rev. B **57**, 15 219 (1998); Y.-N. Xu, Z. Q. Gu, and W. Y. Ching, *ibid.* **56**, 14 993 (1997).
[32] Y.-N. Xu, Z.-Q. Gu, X.-F. Zhong, and W. Y. Ching, Phys. Rev. B **56**, 7277 (1997); W. Y. Ching, Y.-N. Xu, and M. Ruhle, J. Am. Ceram. Soc. **80**, 3199 (1997).
[33] Y.-N. Xu and W. Y. Ching, Phys. Rev. B **59**, 10 530 (1999); *ibid.* **59**, 12 815 (1999).
[34] S. D. Mo, L. Ouyang, W. Y. Ching, I. Tanaka, Y. Koyama, and R. Riedel, Phys. Rev. Lett. **83**, 5046 (1999).
[35] J. Bruley, M.-W. Tseng, and D. B. Williams, Microsc. Microanal. Microstruct. **6**, 1 (1995).
[36] D. Li, M.-S. Peng, and T. Murata, Can. Mineral. **37**, 199 (1999).
[37] Y.-N. Xu and W. Y. Ching, Phys. Rev. B **43**, 4461 (1991).
[38] E. Batkilin, S. Dorfman, and J. Felsteiner, Phys. Lett. A **192**, 273 (1994).
[39] See, for example, F. Aryasetianwan and O. Gunarsson, Rep. Prog. Phys. **61**, 237 (1998), and references cited therein.
[40] See, for example, *Density Functional Theory*, edited by R. F. Nalewajski, Topics in Current Chemistry, Vol. 181 (Springer-Verlag, Berlin, 1996).